Dual Effect of ATP in the Activation Mechanism of Brain Ca^{2+}/Calmodulin-Dependent Protein Kinase II by Ca^{2+}/Calmodulin†

Katalin Török,*,‡ Athanasios Tzortzopoulos,‡ Zenon Grabarek,§ Sabine L. Best,‡ and Richard Thorogate‡

Department of Pharmacology and Clinical Pharmacology, St. George's Hospital Medical School, London SW17 0RE, U.K., and Boston Biomedical Research Institute, Watertown, Massachusetts 02472

Received May 4, 2001; Revised Manuscript Received October 3, 2001

ABSTRACT: The activation mechanism of Ca^{2+}/calmodulin-dependent protein kinase II (αCaMKII) is investigated by steady-state and stopped-flow fluorescence spectroscopies. Lys_{75}-labeled TA-cal [Török, K., and Trentham, D. R. (1994) *Biochemistry 33*, 12807−12820] is used to measure binding events, and double-labeled AEDANS,DDP-T34C/T110/C-calmodulin [Drum et al. (2000) *J. Biol. Chem. 275*, 36334−36340] (DA-cal) is used to detect changes in calmodulin conformation. Fluorescence quenching of DA-cal attributed to resonance energy transfer is related to the compactness of the calmodulin molecule. Interprobe distances are estimated by lifetime measurements of Ca^{2+}/DA-cal in complexes with unphosphorylated nucleotide-free, nucleotide-bound, and Thr_{286}-phospho-αCaMKII as well as with αCaMKII-derived calmodulin-binding peptides in the presence of Ca^{2+}. These measurements show that calmodulin can assume at least two spectrally distinct conformations when bound to αCaMKII with estimated interprobe distances of 40 and 22−26 Å. Incubation with ATP facilitates the assumption of the most compact conformation. Nonhydrolyzable ATP analogues partially replicate the effects of ATP, suggesting that while the binding of ATP induces a conformational change, Thr_{286}-autophosphorylation is probably required for the transition of calmodulin into its most compact conformer. The rate constant for the association of Ca^{2+}/TA-cal with αCaMKII is estimated as 2×10^7 M^{-1} s^{-1} and is not substantially affected by the presence of ATP. The rate of net calmodulin compaction measured by Ca^{2+}/DA-cal is markedly slower, occurring with a rate constant of 2.5×10^6 M^{-1} s^{-1}, suggesting that unproductive complexes may play a role in the activation mechanism.

Ca^{2+}/calmodulin-dependent protein kinase II isozymes (CaMKIIs)[1] are signaling molecules downstream of Ca^{2+}/calmodulin in eukaryotic cells (*1* and references cited within). Upon neurotransmitter stimulus, αCaMKII is translocated to postsynaptic densities in hippocampal slices (*2*) and neurons (*3*). At the postsynaptic densities, αCaMKII catalyzes the phosphorylation of glutamate receptors (*4*) with the effect of changing the ion conductance of these channels (*5*). αCaMKII function is important for the onset of long-term potentiation (*6*), a paradigm for long-lasting changes to synaptic strength (*7*). αCaMKII has a role in spatial learning as demonstrated by experiments with transgenic mice deficient in αCaMKII (*8*). The role of αCaMKII in learning and memory is attributed to its function as a processor in the Ca^{2+}/calmodulin signaling pathway. Although homologous in the catalytic and autoinhibitory domain with other protein kinases (*9*), CaMKIIs have special features. αCaMKII is organized into dodecamers by the stacking of two six-membered rings formed by the C-terminal association domain of each monomer (*10*−*13*). The catalytic domains appear to point outward on a single plane (*13, 14*), but an alternative arrangement in which they stem from the top and bottom of a cylinder has also been put forward (*12*). Another special feature of αCaMKII is Ca^{2+}/calmodulin-dependent autophosphorylation of the Thr_{286} residue which resides in the autoinhibitory domain. Thr_{286}-autophosphorylated αCaMKII (αCaMKII-Thr_{286}-P) 'traps' calmodulin (*15, 16*) and is thought to generate a Ca^{2+}-independently active enzyme (*17, 18*).

In calmodulin, two globular Ca^{2+}-binding lobes are connected by a flexible linker (*19*). When Ca^{2+}/calmodulin is bound to the target peptide derived from αCaMKII, the

† This work is supported by Wellcome Trust Grant 048458 and MRC Grant G9803105 to K.T.

* Correspondence should be addressed to this author at the Department of Pharmacology and Clinical Pharmacology, St. George's Hospital Medical School, Cranmer Terrace, London SW17 0RE, U.K. Phone: +44 208 725 5625; Fax: +44 208 725 3581; E-mail: k.torok@sghms.ac.uk.

‡ St. George's Hospital Medical School.

§ Boston Biomedical Research Institute.

[1] Abbreviations: ADP, adenosine 5′-diphosphate; AMP-PNP, 5′-adenylyl imidodiphosphate; ATP, adenosine 5′-triphosphate; αCaMKII, calmodulin-dependent α protein kinase II; αCaMKII-Thr_{286}-P, Thr_{286}-phospho-αCaMKII; DA-calmodulin, DDP-maleimide- and AEDANS-substituted T34C,T110C-calmodulin; DDP-maleimide, *N*-[4-(dimethylamino)-3,5-dinitrophenyl]maleimide; DTT, 1,4-dithiothreitol; EDTA, ethylenediamine-*N*,*N*,*N*′,*N*′-tetraacetic acid; EGTA, 1,2-bis(2-aminoethoxy)ethane-*N*,*N*,*N*′,*N*′-tetraacetic acid; FRET, fluorescence resonance energy transfer; HPLC, high-pressure liquid chromatography; IAEDANS, 5-[[2-[(iodoacetyl)amino]ethyl]amino]naphthalene-1-sulfonic acid; LDH, lactate dehydrogenase; MLC, chicken gizzard smooth muscle myosin light chain; MLCK, smooth muscle myosin light chain kinase; NADH, reduced nicotinamide adenine dinucleotide; PBS, phosphate-buffered saline, pH 7.4; PEP, phosphoenolpyruvate; PIPES, piperazine-*N*,*N*′-bis(2-ethanesulfonic acid); PK, pyruvate kinase; PMSF, phenylmethylsulfonyl fluoride; TA-calmodulin or TA-cal, 2-chloro-(ϵ-amino-Lys_{75})-[6-(4-*N*,*N*-diethylaminophenyl)-1,3,5-triazin-4-yl]calmodulin; TA-Cl, 2,4-dichloro-6-(4-*N*,*N*-diethylaminophenyl)-1,3,5-triazine; TFA, trifluoroacetic acid; Tris, tris(hydroxymethyl)aminomethane.

10.1021/bi010920+ CCC: $20.00
Published on Web 11/15/2001

linker 'collapses', and the distance between the two Ca^{2+}-binding lobes is greatly reduced (*19*−*21*). This process can be monitored by the fluorescent calmodulin derivative DA-cal which reports the distance between the two Ca^{2+}-binding lobes of calmodulin by fluorescence energy transfer. The spectral overlap of AEDANS emission and DDP absorption has been utilized before in demonstrating distance changes between two Cys residues in a myosin fragment associated with ADP trapping (*22*). This chromophore pair was used to label a calmodulin double-mutant (C34T/C110T-calmodulin) so that the fluorescent donor (AEDANS) is located on one of the lobes and the acceptor (DDP) probe resides on the other lobe of the molecule (*23*−*25*). In the resulting AEDANS,DDP-C34T/C110T-calmodulin, termed DA-cal, fluorescence intensity is dependent on the distance between the donor and acceptor, and quenching of the donor fluorescence corresponds to a decrease in distance between the two Ca^{2+}-binding lobes. Using DA-cal, it has been demonstrated that Ca^{2+}/calmodulin adopts extended conformations with caldesmon and a bacterial adenylyl cyclase (*23*, *25*) and that Ca^{2+}/calmodulin conformation is compact in complex with MLCK and MLCK-derived calmodulin-binding peptide (*24*). These studies show that DA-cal accurately reports variations in calmodulin conformation corresponding to the distance between its Ca^{2+}-binding lobes. The conformation of the double-labeled calmodulin can be monitored by measurement of either the fluorescence intensity or the lifetime of the donor. A second fluorescent calmodulin, TA-cal, a Lys_{75}-labeled derivative, responds to Ca^{2+} and target binding with fluorescence changes (*26*, *27*). TA-cal has been applied to determining the kinetic mechanism of its interaction with MLCK and peptides and for imaging of calmodulin activation during mitosis (*26*, *28*, *29*). Using these two fluorescent calmodulin probes, here we report a study of the mechanism of Ca^{2+}/calmodulin activation of αCaMKII.

MATERIALS AND METHODS

Vectors. αCaMKII was obtained by overexpression in baculovirus (kindly provided by Dr. D. A. Brickey and Professor T. R. Soderling, Portland, OR) transfected Sf9 insect cells. The plasmid pVL1393 containing the cDNA for the expression of rat αCaMKII was cotransfected with a linearized baculovirus DNA (BaculoGold, PharMingen) into Sf9 cells using Lipofectin (Gibco Life Technologies).

Expression and Purification of αCaMKII. Overexpression of αCaMKII in baculovirus-transfected insect cells was utilized so that a single isoform could be studied. Using a single isoform and a homogeneous protein population is advantageous in mechanistic studies. The expression system, developed by Brickey et al. (*30*), provides oligomerically folded αCaMKII (*11*−*13*). For αCaMKII expression, 1.8×10^7 Sf9 cells in a T225 flask were transfected with the recombinant virus at 10:1 multiplicity of infection (moi) and incubated at 28 °C for 72 h. Typically the yield was ∼0.75 mg of αCaMKII/1.8×10^7 cells. The cells were harvested by centrifugation at 1000*g* for 10 min at 21 °C. The cell pellet was resuspended in 2 mL of PBS, pH 7.4, containing 2 mM DTT, 0.5 mM PMSF, 0.1 mM $CaCl_2$, 400 μM leupeptin, 73 μM pepstatin. The cells were lysed by three repeated cycles of freezing in liquid nitrogen and thawing at 42 °C. The cell lysate was centrifuged at 35000*g* for 20 min at 4 °C. The supernatant of the cell lysate was loaded onto a 10 mL calmodulin−Sepharose (Pharmacia) column equilibrated with buffer A (20 mM Tris·HCl, pH 7.5, 1 mM $CaCl_2$, 1 mM DTT, 0.1 mM PMSF, 8 μM leupeptin, 1.5 μM pepstatin), and αCaMKII was eluted with buffer B (20 mM Tris·HCl, pH 7.5, 2 mM EGTA, 1 mM DTT, 0.1 mM PMSF, 8 μM leupeptin, 1.5 μM pepstatin). The eluted protein was applied to a Mono Q HR 10/10 FPLC column (Pharmacia) equilibrated with buffer B. An 80 mL gradient (0−1 M NaCl) was applied; αCaMKII eluted at 450 mM NaCl. The protein was electrophoretically homogeneous (Figure 1C, lane 2). The fractions were rapidly frozen in liquid nitrogen for storage at −80 °C.

Synthesis of DA-cal. Human liver calmodulin c-DNA was the gift of Dr. R. Perham (Cambridge, U.K.). AEDANS/DDP-34/110-calmodulin was prepared as follows (*25*): human liver calmodulin c-DNA was subcloned into pAED4 vector [gift of Dr. D. S. Doering (Cambridge, MA)] at *Nde*I for the 5′ end and at *Pst*I for the 3′ end. Polymerase chain reaction was used to substitute Cys for Thr110 using primers 5′-CAC GTC ATG TGC AAC TTA GGA G-3′ and 5′-TCC TAA GTT GCA CAT GAC GTG-3′. Cys substitution of Thr34 of the T110C mutant was then carried out using primers 5′-GAA CTT GGA TGC GTC ATG AGG-3′ and 5′-CCT CAT GAC GCA TCC AAG TTC C-3′. Mutant calmodulin was expressed in BL21-Gold (DE3) cells (Stratagene) and purified from the soluble fraction of the cell lysate by Phenyl-Sepharose and Mono Q (Pharmacia) chromatography. For double-labeling, mutant calmodulin was first incubated in 25 mM Na^+-HEPES, pH 7.5, 100 mM NaCl, 0.1 mM EGTA with 0.4 equiv of IAEDANS for 12 h at 4 °C. To this mixture was added a 1.5-fold excess of DDP-maleimide, and further incubation was carried out for 12 h at 4 °C. In addition to the target derivatives C34-AEDANS/C110-DDP and C34-DDP/C110-AEDANS-calmodulin (together termed DA-cal), the reaction mixture was expected to contain unlabeled C34T/C110T-calmodulin, singly labeled AEDANS- and DDP-maleimide derivatives, and double-labeled C34-AEDANS/C110-AEDANS and C34-DDP/C110-DDP-calmodulin as well. The reaction mixture was separated by reverse-phase HPLC using a H_2O-acetonitrile gradient containing TFA (0.082% in the aqueus solvent and 0.1% in the organic solvent). The labeled species were identified by monitoring DDP absorption at 442 nm and AEDANS fluorescence at 340 nm excitation and 500 nm emission. Typically five peaks were observed; elution of residual unlabeled calmodulin was followed by AEDANS-cal, then AEDANS/DDP-cal (DA-cal) in two peaks and DDP-cal. Desalted and lyophilized DA-cal fractions were screened to select those in which maximum donor quenching occurred by αCaMKII peptide binding.

Characterization of DA-cal. DA-cal obtained by HPLC purification of the double-labeled bacterially expressed C34T/C110T-calmodulin double-mutant was characterized with respect to its purity, composition, target binding properties, and stimulation of steady-state αCaMKII activity and Thr_{286}-autophosphorylation. Matrix-assisted laser-desorption ionizing time-of-flight (maldi-tof) mass and sequence analyses were carried out at Kratos Analytical, Manchester, U.K. The molecular mass of the T34C/T110C mutant was 16 711 Da (for 16 710.5 Da calculated mass), confirming the structure of the bacterially overexpressed human calmodulin double-

mutant. This mass was 4.0 Da larger than that for the wild-type calmodulin, as predicted. The mass of DA-cal was measured as 17 315 Da (within 8 Da of the theoretical mass of 17 323 Da). DA-cal was further analyzed by identifying peptides 31−37 and 107−115 and their labeled equivalents in tryptic digests of the double-mutant and of DA-cal, respectively. The correct masses for peptides corresponding to residues 31−37 (804.4 Da) and 107−115 (1027.5 Da) were identified in the digest of unlabeled double-mutant. In the digest of DA-cal, the respective derivatized peptides were identified (1113.4 and 1336.6 Da, respectively), and their labeling was confirmed by sequence analysis in maldi-tof mass spectrometry, although the mass difference of 0.2 Da between the AEDANS moiety (306.2 Da) and the DDP-maleimide adduct (306.4 Da) was too small to further assess the distribution of the two probes on C_{34} and C_{110}. Our detailed analysis thus showed specific labeling and homogeneity of DA-cal.

Binding Affinity of Ca^{2+}/DA-cal to αCaMKII Peptide. The target binding affinity of Ca^{2+}/DA-cal for the Ac-294−309-NH_2 peptide was compared with that of unmodified calmodulin purified from pig brain by equilibrium competition (*26*). Ca^{2+}/DA-cal fluorescence was measured in a mixture of Ca^{2+}/DA-cal and excess peptide to which aliquots of pig brain Ca^{2+}/calmodulin were added to displace Ca^{2+}/DA-cal. The fluorescence reading at each point gave the concentrations of peptide-bound and free Ca^{2+}/DA-cal as well as defined the concentration of peptide-bound Ca^{2+}/cal and, thus, that of free Ca^{2+}/cal. From the plot of these data, the ratio of dissociation constants, K_d(cal)/K_d(DA-cal) = 1.9, was determined for the Ac-294−309-NH_2 peptide. Thus, the target binding affinity of Ca^{2+}/DA-cal was comparable to that of Ca^{2+}/calmodulin.

Enzyme Activity. Steady-state protein kinase activity of αCaMKII stimulated by calmodulin and DA-calmodulin was measured using the regulatory light chain of chicken gizzard myosin MLC (see below for source and quantitation) as target. A continuous enzyme-linked fluorescence assay was used to determine ADP production linked to NADH oxidation with a 1:1 stoichiometry (*31*). The reactions were carried out at 21 °C. The 0.5 mL assay solution contained 50 mM K^+-PIPES, pH 7.0, 100 mM KCl, 5 mM DTT, 2 mM $MgCl_2$, 2 mM PEP, 500 μM $CaCl_2$, 4.5 units of LDH (bovine heart), 2 units of PK (rabbit muscle), 10.8 μM NADH. The concentrations of ATP, calmodulin, and MLC were varied as specified. λ_{ex} was 340 nm. λ_{em} was set to 420 nm where DA-cal emission was negligible. DA-cal and pig brain calmodulin were compared in steady-state assays of phosphorylation of the target MLC by αCaMKII. In the continuous fluorescence coupled assay described above, at 1 mM ATP, 50 μM MLC, 160 nM αCaMKII (M_w 54 325), 1.8 μM calmodulin or DA-cal, the specific activities were 525 and 451 nmol of ADP min^{-1} (mg of αCaMKII)$^{-1}$, corresponding to k_{cat} values of 0.48 s^{-1} for activation by DA-cal and 0.41 s^{-1} in the case of pig brain calmodulin.

Activation of Thr_{286}-Autophosphorylation of αCaMKII by Ca^{2+}/Calmodulin and Ca^{2+}/DA-cal. αCaMKII (0.74 μM), 1 μM pig brain calmodulin or DA-calmodulin, and 0.25 mM ATP were incubated in 50 mM PIPES (K^+ salt), pH 7.0, 100 mM KCl, 2 mM $MgCl_2$, 1 mM DTT, and 500 μM $CaCl_2$ at 21 °C for various times up to 120 s. The reaction was terminated by SDS sample-buffer. Western blotting with anti-phospho-Thr_{286}-αCaMKII was carried out as described below. The time-course was assessed by densitometry of Western blots. An Alpha Innotech Corp. densitometer with Fluorchem v 2.00 software was used. Densities up to 30% were proportionate to loaded protein.

Western Blotting. Western blotting was carried out by the method of Towbin et al. (*32*). Anti-αCaMKII mouse monoclonal and anti-phospho-Thr_{286}-αCaMKII mouse monoclonal antibodies were used to detect Thr_{286}-autophosphorylation by calmodulin and DA-cal. Protein samples were separated on gradient SDS−polyacrylamide gels and transferred to a nitrocellulose membrane equilibrated in Towbin transfer buffer (25 mM Tris, 192 mM glycine, containing 20% methanol, pH 8.3), using a semi-dry electrophoretic transfer cell for 35 min at 80 mA. After incubation with 5% nonfat milk in PBS for 15 min, membranes were incubated with mouse monoclonal anti-phospho-αCaMKII (Upstate Biotechnology) (final antibody concentration 1 μg/mL) and anti-αCaMKII (Boehringer Mannheim, final antibody concentration 0.5 μg/mL) antibodies for 12 and 3 h, respectively. Membranes were then incubated with alkaline phosphatase conjugated secondary antibodies for 2 h, and bound antibodies were visualized by colorimetric detection with the Nitroblue tetrazolium chloride (NBT)/5-bromo-4-chloro-3-indolyl phosphate (BCIP) color detection system (Boehringer Mannheim) followed by washing with TE buffer (10 mM Tris-HCl, pH 8.0, 1 mM EDTA).

Other Proteins and Peptides. Pig brain calmodulin was purified as previously described (*26*) and was used in stopped-flow and equilibrium competition experiments to displace DA-cal. TA-cal was synthesized as previously described (*26*). MLC was used as αCaMKII target as αCaMKII catalyzes the phosphorylation of Ser_{19} of MLC (*33*). A previously developed high-yield MLC expression system in BL21-Gold (DE3) cells (Stratagene) was utilized, and purification was carried out as described in (*34*); 270 mg of MLC was purified from a 3 L culture. αCaMKII-derived peptides corresponding to residues Ac-294−309-NH_2 (Ac-NARRKLKGAILTTMLA-NH_2) and 281−319 (MHRQ-ETVDCLKKFNARRKLKGAILTTMLATRNFSGGKGG) and its analogue, 281−319-Thr_{286}-P, were synthesized by f-moc chemistry and purified to homogeneity by reverse-phase HPLC with a gradient (0.5% change/min) of 0.1% TFA in H_2O to 0.082% TFA in CH_3CN on a Waters Deltapak C_{18} column (30 mm × 30 cm) at a flow rate of 2.0 mL/min. The molecular masses (theoretical values in parentheses) were determined by electrospray mass spectrometry as 1797 Da (1798.2 Da), 4332.8 Da (4336.1 Da), and 4418.5 Da (4416.1 Da), respectively, confirming the peptide structures. Electrospray mass spectroscopy was carried out by Dr. S. A. Howell at NIMR, London, U.K.

Protein and Peptide Concentration Measurements. The concentration of αCaMKII was measured using ϵ_o = 64 805 M^{-1} cm^{-1} (280 nm) calculated from the amino acid composition (*35*). The Bradford assay was also used with BSA as standard (*36*). The results of the two protein assays were consistent within 10%. The value ϵ_o = 1800 M^{-1} cm^{-1} (278 nm) in 2 mM EGTA was used for pig brain calmodulin and T34C/T110C-calmodulin, and for MLC, ϵ_o = 4400 M^{-1} cm^{-1} (278 nm) was calculated from the amino acid composition (*35*). DA-cal protein concentration was measured by Bradford assay using T34C/T110C-calmodulin as standard.

For estimation of stoichiometry of labeling, $\epsilon_o = 6100\ M^{-1}\ cm^{-1}$ (337 nm) for the AEDANS and $\epsilon_o = 2930\ M^{-1}\ cm^{-1}$ (442 nm) for the DDP moiety were used (*22*). Peptide concentrations were determined by weight and quantitative amino acid analysis and are accurate with a 10% error of measurement.

Determination of the R_o for DA-cal (37). Steady-state fluorescence measurements were carried out to determine the values for the donor quantum yield in the absence of the acceptor, Q_D, and the overlap integral, J_{DA}, for DA-cal using an SLM spectrofluorometer (*37*). Corrected emission spectra were generated using quinine sulfate in 0.5 M H_2SO_4 and its true spectrum (Molecular Probes). The excitation wavelength was 347 nm. Donor quantum yields of AEDANS-T34C/T110C-calmodulin in different solution and liganded conditions were determined relative to that of quinine sulfate of 0.55 in 0.5 M H_2SO_4 using the relationship: $Q_D = Q_{ref}F_DA_{ref}/F_{ref}A_D$, where the quantum yield Q is expressed as a function of the areas under the corrected emission spectra F and the absorption values at the excitation wavelength A for two fluorescent compounds. The areas were calculated from fluorescence intensities measured at 0.2 nm intervals. The optical density of the chromophore solutions was <0.03 at the excitation wavelength.

In each solution condition, the spectral overlap between the corrected emission spectrum of AEDANS-T34C/T110C-calmodulin and the absortion spectrum of the β-mercaptoethanol adduct of DDP-maleimide was determined to give the overlap integral, J_{DA} (*37*). The DDP absorption spectrum was not affected by calmodulin labeling.

Lifetime measurements were carried out on a modified ORTEC 9200 nanosecond fluorometer and an IBH system (Glasgow, U.K.) using a pulsed N_2 (338 nm) or nanoLED (370 nm) source, and data were acquired by time-correlated single-photon counting. Fluorescence decay curves were fit with exponentials, and lifetimes were determined by the method of moments procedure (*38*). Distances (R) between the donor and acceptor probes were calculated from the lifetimes using the relationships: $R = R_o[(1 - E)/E - 1]^{1/6}$ and $\tau_{DA}/\tau_D = 1 - E$ where τ_{DA} and τ_D represent the donor lifetime in the presence and absence of acceptor, respectively, as given by the Förster theory of resonance energy transfer (*37*).

Other Spectroscopy. Experiments were carried out at 21 °C unless otherwise specified. The assay solution contained 50 mM PIPES (K^+ salt), pH 7.0, 100 mM KCl, 2 mM $MgCl_2$, 1 mM DTT, and 500 μM $CaCl_2$, unless otherwise stated. Fluorescence stopped-flow measurements were carried out using a Hi-Tech PQ/SF-53 double-mixing apparatus (Hi-Tech Scientific, U.K.) set to $\lambda_{ex} = 363$ nm and $\lambda_{em} > 455$ nm for experiments with DA-cal. A Varian spectrophotometer, an SLM spectrofluorometer, and a SPEX Fluorolog 2/2/2 photon-counting fluorometer were used for absorption and other fluorescence measurements.

Software. Hi-Tech RK-2 program and GRAFIT 4 were used to acquire and analyze the kinetic data. KSIM (by Neil Millar) was used to generate simulated kinetic reactions. BINDPC (developed by Dr. E. P. Morris) was used to determine equilibrium binding constant of DA-cal and αCaMKII.

RESULTS

Steady-State Fluorescence of Ca^{2+}/DA-cal in αCaMKII Complexes. Steady-state fluorescence emission intensities of Ca^{2+}/DA-cal free in solution were compared with those of Ca^{2+}-free DA-cal, Ca^{2+}/DA-cal in complex with αCaMKII in the presence and absence of ATP, and that in complex with αCaMKII peptide Ac-294−309-NH_2. As seen in Figure 1A, the fluorescence intensity of DA-cal was the highest in the presence of EGTA. The fluorescence of Ca^{2+}/DA-cal was lower, and αCaMKII binding caused further quenching of Ca^{2+}/DA-cal fluorescence. Maximal quenching to 18% of the fluorescence of free Ca^{2+}/DA-cal was observed both with αCaMKII in the presence of ATP and with the Ac-294−309-NH_2 peptide. As the reported dissociation constant for the complex of αCaMKII is relatively high, 45 nM (*16*), it was important to check that αCaMKII binding to Ca^{2+}/DA-cal was saturated. Thus, equilibrium binding measurements were carried out. These showed that the fluorescence of Ca^{2+}/DA-cal in the presence of saturating αCaMKII ($\geq 6.4\ \mu$M) was 70% of that of free Ca^{2+}/DA-cal (Figure 1B). As seen in Figure 1C,D, Thr_{286}-autophosphorylation occurs when αCaMKII, Ca^{2+}/DA-cal, and ATP are incubated together. Thr_{286}-autophosphorylation of αCaMKII thus appears to be associated with enhanced fluorescence quenching of Ca^{2+}/DA-cal. These data show that spectroscopically different complexes of Ca^{2+}/DA-cal are formed with nucleotide-free αCaMKII compared to that with Thr_{286}-autophosphorylated αCaMKII. Furthermore, the complex formed with the Ac-294−309-NH_2 peptide is spectroscopically similar to that with Thr_{286}-autophosphorylated αCaMKII.

Fluorescence Lifetime Measurements of Ca^{2+}/DA-cal Conformation in αCaMKII Complexes. The probes AEDANS and DDP attached to T34C/T110C-calmodulin form a resonance energy transfer pair; thus, the differences in the AEDANS fluorescence emission spectra of DA-cal can be related to differences in the distance between the donor and acceptor probes. To monitor the interprobe distance in the αCaMKII and peptide complexes of Ca^{2+}/DA-cal, first the critical distance R_o was estimated for DA-cal in the different complexes. R_o values were calculated as described under Materials and Methods from the measurements of the quantum yield and the overlap integral in each condition. As shown in Table 2, the estimated R_o value for both Ca^{2+}-free and Ca^{2+}-bound DA-cal was 26 Å, a value similar to that estimated for a myosin fragment labeled with these probes (*22*). Minor changes to the quantum yield and the overlap integral caused by αCaMKII or peptide binding resulted in a ≤ 0.5 Å increase in the value of R_o (Table 1).

As a basis for distance estimation by energy transfer, fluorescence lifetime measurements were made of donor-only labeled AEDANS-C34T/C110T-calmodulin and of its complexes with αCaMKII, αCaMKII-Thr_{286}-P, and Ac-294−309-NH_2 peptide. The decay of AEDANS-C34T/C110T-calmodulin fluorescence was in each case well fit to a single exponential. The lifetime of AEDANS-C34T/C110T-calmodulin was 12 ns in the absence and 13 ns in the presence of Ca^{2+}, but was somewhat longer, 15 ns, in the αCaMKII and peptide complexes.

Lifetime measurements of donor- and acceptor-labeled DA-cal were then carried out. The fluorescence decay of Ca^{2+}-free DA-calmodulin was monoexponential with a lifetime of 11.4 ns, corresponding to a slight reduction compared to donor-only labeled calmodulin (Table 1 and Figure 1E). In the presence of Ca^{2+}, however, the fluorescence decay of free Ca^{2+}/DA-cal in solution could be best

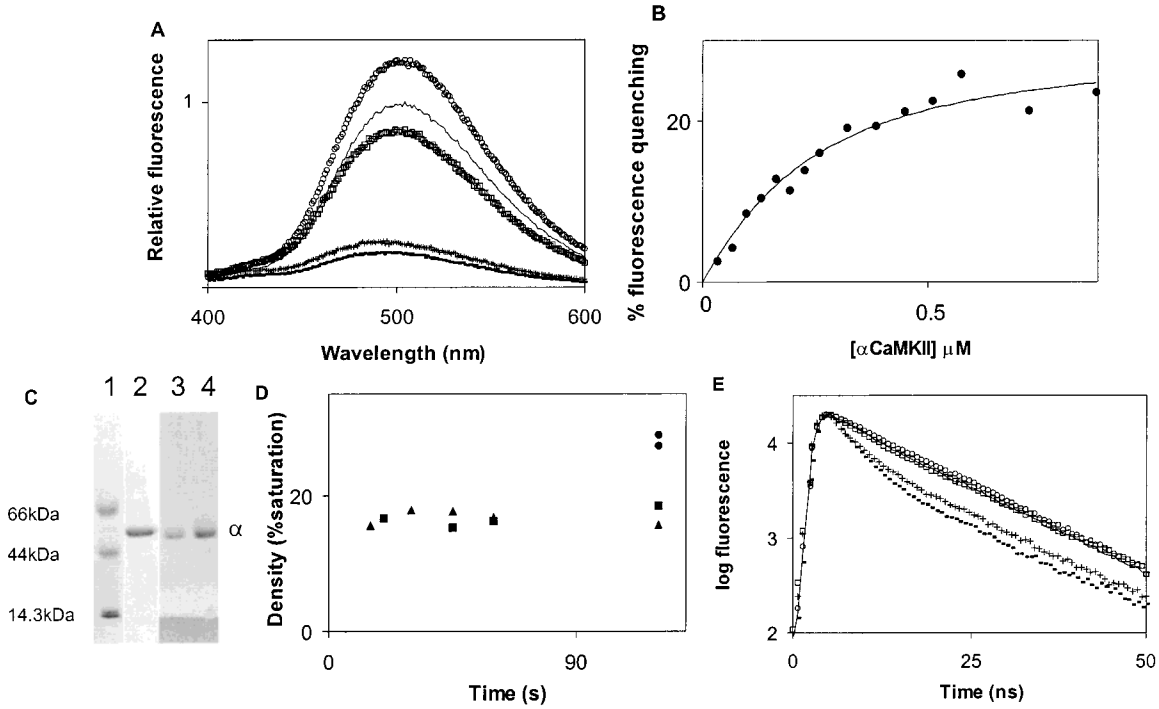

FIGURE 1: Resonance energy transfer measurements of complexes of AEDANS,DDP-34,110-calmodulin (DA-cal) and αCaMKII by equilibrium fluorescence and lifetime measurements. Fluorescence of Ca^{2+}/DA-cal is defined as unity, 1, and that of buffer is 0. (A) Emission spectra of the following complexes at 1.15 μM DA-cal and 1 μM αCaMKII or peptide were recorded (relative fluorescence in parentheses): DA-cal in 0.4 mM EGTA (1.23) (○); DA-cal in 0.6 mM Ca^{2+} (1) (—); DA-cal and αCaMKII in 0.1 mM Ca^{2+} (0.85) (□); DA-cal, αCaMKII, and 0.5 mM ATP in 0.1 mM Ca^{2+} (0.25) (+); αCaMKII peptide and DA-cal in 0.6 mM Ca^{2+} (0.19) (- - -). Excitation wavelength was at 335 nm. Comparison of the emission spectra of donor-only labeled AEDANS-T34C/T110C-calmodulin in these conditions showed that Ca^{2+} binding did not affect the emission spectrum in the range of $10^{-8}-10^{-3}$ M free Ca^{2+} concentration. A blue shift of 10 nm and an intensity increase by 9% at 500 nm were induced by the binding of αCaMKII peptide to AEDANS-T34C/T110C-calmodulin. Both αCaMKII and αCaMKII-Thr_{286}-P binding to AEDANS-T34C/T110C-calmodulin caused a blue shift of 10 nm. (B) Measurement of the dissociation constant for Ca^{2+}/DA-cal and αCaMKII by equilibrium binding. 80 nM Ca^{2+}/DA-cal was titrated with aliquots of a 14 μM stock solution of αCaMKII in 500 μL. Maximum quenching of Ca^{2+}/DA-cal fluorescence was 30% (to give relative fluorescence 0.7). Best fit for K_d was 97 (±5) nM. (C) Purity and Thr_{286}-autophosphorylation of αCaMKII. SDS−PAGE of molecular mass markers (5 μg of each protein) (lane 1) and purified αCaMKII (8 μg) (lane 2). Thr_{286}-autophosphorylation was detected by Western blotting using anti-phospho-Thr_{286}-αCaMKII as described under Materials and Methods. In lanes 3 and 4, Western blot of two different protein loads is shown. Samples were taken from the autophosphorylation mixture stimulated by calmodulin at 120 s. Aliquots containing 0.34 and 0.68 μg of αCaMKII were loaded in lanes 3 and 4, respectively. (D) Time-course of Thr_{286}-autophosphorylation analyzed by densitometry of Western blots. The plateau of density was reached by 20 s and was 16.8% (±1.3) and 17% (±1) for calmodulin (■) and DA-cal (▲), respectively. With double amounts of protein loaded (●, duplicate samples), the density was 29% (±2). With T286A mutant, no staining was detected with anti-phospho-Thr_{286}-αCaMKII (not shown). Thr_{286}-autophosphorylation was complete within 20 s by both Ca^{2+}/DA-cal and Ca^{2+}/calmodulin stimulation. Thus, αCaMKII was Thr_{286}-autophosphorylated in the presence of ATP and Ca^{2+}/DA-cal on the time-scale of our steady-state experiments. (E) Fluorescence lifetime measurements in complexes of Ca^{2+}/DA-cal and αCaMKII. The same samples were used as described in panel A: (○) DA-cal in 0.4 mM EGTA [τ_{da1}, 11.4 ns; A_1, 1; distance (da1), 39 Å]; (—) DA-cal in 0.6 mM Ca^{2+} [τ_{da1}, 12.5 ns; A_1, 0.56; distance (da1), 50 Å; τ_{da2}, 7.9 ns; A_2, 0.44; distance (da2), 28 Å]; (□) DA-cal and αCaMKII in 0.1 mM Ca^{2+} [τ_{da1}, 14.2 ns; A_1, 0.39; distance (da1), 45 Å; τ_{da2}, 7.9 ns; A_2, 0.61; distance (da2), 27 Å]; (+) DA-cal, αCaMKII, and 0.5 mM ATP in 0.1 mM Ca^{2+} [τ_{da1}, 14.2 ns; A_1, 0.25; distance (da1), 40 Å; τ_{da2}, 5.0 ns; A_2, 0.75; distance (da2), 23 Å]; (- - -) αCaMKII peptide Ac-294−309-NH_2 and DA-cal in 0.6 mM Ca^{2+} [τ_{da1}, 13.7 ns; A_1, 0.16; distance (da1), 41 Å; τ_{da2}, 4.2 ns; A_2, 0.84; distance (da2), 23 Å]. Excitation wavelength was at 335 nm.

fit with two exponentials. In addition to the component with 11.9 ns lifetime, a shorter component of 5.7 ns appeared representing 25% of the amplitude. Interestingly, similar lifetimes, 14.1 and 6.7 ns, were observed in the complex with αCaMKII; however, the shorter lifetime was more abundant in the αCaMKII complex representing 52% of the amplitude. In the complex of Ca^{2+}/DA-cal with αCaMKII-Thr_{286}-P, the major lifetime component was 3.8 ns, representing 80% of the amplitude; 20% of the fluorescence appeared to be unquenched. A similar observation was made in the complex with the Ac-294−309-NH_2 peptide, where the 3.8 ns lifetime component represented 85% of the amplitude with 15% of the fluorescence remaining unquenched.

The fluorescence decay of DA-cal was monoexponential in EGTA; however, in all the other conditions, the decay was best fit with two exponentials. The biexponential nature of the DA-cal fluorescence decay in the context of monoexponential decay of the donor-only labeled calmodulin fluorescence can be explained by the presence of two calmodulin conformers with different interprobe distances. Interprobe distances were calculated from the ratio of the lifetimes measured in donor-only labeled calmodulin and that in donor−acceptor-labeled calmodulin (Table 1). Ca^{2+}-free DA-cal appears to exist as a single conformer with a 39 Å interprobe distance. In contrast, two Ca^{2+}/DA-cal conformers are detected with estimated interprobe distances of 40 and 28 Å (Figure 1E and Table 1). In complex with αCaMKII, the decay of Ca^{2+}/DA-cal fluorescence was also biexponential, and the two lifetimes corresponded to interprobe distances of 44 and 26 Å (Table 1). These data suggest that Ca^{2+}/DA-cal exists in two conformations both in complex

Table 1: Donor−Acceptor Distances of Ca^{2+}/DA-cal in Complexes with αCaMKII, αCaMKII-Thr_{286}-P, and αCaMKII Peptide Ac-294−309-NH_2[a]

reactant	Q_D	J_{DA} ($M^{-1}cm^{-1}$ nm)	R_o (Å)	$\tau_{(d)}$ (ns) (sd) χ^2/n[d]	$\tau_{1(da)}$ (ns) (sd) χ^2/n[d]	A_1 (sd)	E_1 (sd)	distance (da_1) (Å) (sd)	$\tau_{2(da)}$ (ns) (sd)	A_2 (sd)	E_2 (sd)	distance (da_2) (Å) (sd)
EGTA	0.23	8.6×10^{13}	25.9	12.41 (±0.01) ≤2.3	11.44 (±0.03) ≤6.7	1	0.08 (±0.01)	38.9 (±0.2)				
Ca^{2+}	0.23	8.6×10^{13}	25.9	12.73 (±0.13) ≤2.4	11.9 (±0.8) ≤3.4	0.75 (±0.15)	0.07 (±0.02)	40 (±2)	5.7 (±3.3)	0.25 (±0.15)	0.39 (±0.26)	28 (±4)
αCaMKII	0.25	8.9×10^{13}	26.4	14.76 (±0.25) ≤2.1	14.1 (±0.7) ≤7.4	0.48 (±0.08)	0.05 (±0.03)	44 (±3)	6.7 (±1.4)	0.52 (±0.08)	0.55 (±0.10)	26 (±2)
αCaMKIIThr_{286}-P[b]	0.24	9.0×10^{13}	26.3	15.37 (±0.14) ≤4.1	13.6 (±0.5) ≤4.2	0.20 (±0.07)	0.12 (±0.03)	37 (±1)	3.8 (±0.4)	0.80 (±0.07)	0.75 (±0.04)	22 (±1)
αCaMKII peptide Ac-294−309 -NH_2[c]	0.25	8.9×10^{13}	26.4	14.66 (±0.31) ≤7.3	13.7 (±0.2) ≤3.7	0.15 (±0.07)	0.06 (±0.03)	41 (±2)	3.8 (±0.4)	0.85 (±0.07)	0.74 (±0.03)	22 (±1)

[a] Lifetime measurements were carried out in solution conditions described in the legend to Figure 1A,E. Donor quantum yield, Q_D, values were measured as described under Materials and Methods relative to that of quinine sulfate. In the calculation of J_{DA}, the value 0.667 was used for the orientation factor κ^2 and $n = 1.4$ for the refractive index. E_1 and E_2 represent transfer efficiencies corresponding to τ_1 and τ_2, respectively. [b]The residual unquenched component likely represents αCaMKII that remained unphosphorylated as well as some free Ca^{2+}/DA-cal. [c] The amplitude of the unquenched component (0.14) corresponded to the excess of Ca^{2+}/DA-cal over peptide. At least three independent lifetime measurements were made in each condition. [d]The largest χ^2/n value is shown for each condition. The range of values of χ^2/n obtained using the lifetime apparatus and analysis system built by Dr. Terry Tao was similar to previously published data using the same system and corresponded to good fits to the data (*38, 49*). Data collection was optimized for the several nanosecond long AEDANS lifetime; one channel corresponded to 0.67 ns. Values of $\chi^2/n > 3$ in some samples appeared to arise due to scattering with lifetime <1 ns. This component was analyzed as a third exponential in data (not shown) collected at IBH (Glasgow, U.K.) with channel calibration 0.12 ns. Such an analysis did not significantly affect our conclusions drawn from the data shown in Table 1. The χ^2/n values listed in the column for $\tau_{1(da)}$ apply for the whole measurement to which $\tau_{1(da)}$ and $\tau_{2(da)}$ values were fit.

with αCaMKII and free in solution. Moreover, the two measured distances between the probes located in the Ca^{2+}-binding lobes do not change substantially on αCaMKII binding. Thus, the extended Ca^{2+}/DA-cal conformer with 40 Å interprobe distance appears to correspond to the conformer with 44 Å in complex with αCaMKII. The equivalent of the less extended (semi-compact) conformer of Ca^{2+}/DA-cal of 28 Å interprobe distance appeared in the αCaMKII complex with a similar distance of 26 Å. The enhanced quenching by αCaMKII observed in steady-state can be explained by more of the semi-compact Ca^{2+}/DA-cal conformer (52%) being present in complex with αCaMKII than when Ca^{2+}/DA-cal is free in solution (25%).

In the Ca^{2+}/DA-cal complexes with both αCaMKII-Thr_{286}-P and αCaMKII peptide Ac-294−309-NH_2, the dominant lifetime corresponded to a 22 Å interprobe distance (Figure 1E and Table 1). The overall conformation of Ca^{2+}/DA-cal in these complexes can be viewed as compact. Taken together, our energy transfer measurements suggested that ATP caused a transition in the αCaMKII-bound conformation of Ca^{2+}/DA-cal from extended to compact.

Effect of Nucleotides on the Global Conformation of αCaMKII-Bound Ca^{2+}/DA-cal. In the presence of ATP, αCaMKII autophosphorylation is stimulated by Ca^{2+}/DA-cal (see Figure 1C,D) and gives αCaMKII-Thr_{286}-P. Thus, the ATP-induced transition in the global conformation of Ca^{2+}/calmodulin bound to αCaMKII from extended to compact may have been caused either directly by ATP binding or by Thr_{286}-autophosphorylation. We therefore used nonhydrolyzable nucleotides to establish the contribution of nucleotide binding and Thr_{286}-autophosphorylation. All experiments with these compounds showed significant quenching of Ca^{2+}/DA-cal fluorescence. The fluorescence of αCaMKII-bound Ca^{2+}/DA-cal was 57% quenched by AMP-PNP while ADP caused 51% quenching (Table 2). Thus, since the ATP analogues produce substantial quenching, it is likely that a considerable proportion of the total fluorescence quenching induced in the αCaMKII-bound Ca^{2+}/DA-cal by ATP can be ascribed to a direct effect rather than the subsequent autophosphorylation.

Kinetics of Ca^{2+}/DA-cal Interactions with αCaMKII and the Effect of Nucleotides. To understand the mechanism of Ca^{2+}/calmodulin binding to αCaMKII, the kinetics of Ca^{2+}/DA-cal association with and dissociation from nucleotide-free and nucleotide-bound αCaMKII complexes were investigated in fluorescence stopped-flow experiments. Control experiments showed that none of the nucleotides had a direct effect on Ca^{2+}/DA-cal fluorescence by itself. Throughout the experiments, fluorescence was normalized so that relative fluorescence 1 corresponded to Ca^{2+}/DA-cal and 0 to buffer.

The association kinetics of Ca^{2+}/DA-cal were studied with nucleotide-free αCaMKII and with αCaMKII in the presence of ATP and ADP. Figure 2A shows a typical fluorescence stopped-flow record of Ca^{2+}/DA-cal association with nucleotide-free αCaMKII in which the quenching of fluorescence which occurs over seconds can be described by a single exponential (record 1). The observed rate of Ca^{2+}/DA-cal fluorescence change (k_{obs}) was measured as a function of αCaMKII concentration. k_{obs} showed little concentration dependence and appeared to saturate within the αCaMKII concentration range of 5 μM (Figure 2B). In similar stopped-flow experiments when αCaMKII was mixed with ATP and Ca^{2+}/DA-cal, the observed rate of Ca^{2+}/DA-cal fluorescence change showed a linear dependence on αCaMKII concentration with a slope of 2.5×10^6 M^{-1} s^{-1} (Figure 2C). A similar effect was observed when ATP was replaced with ADP (Figure 2C). The rate of fluorescence change showed a similar linear dependence upon αCaMKII concentration; only

Table 2: Kinetic Parameters of the Interactions of Ca^{2+}/DA-cal and Ca^{2+}/TA-cal with αCaMKII and αCaMKII Peptides

(Ca^{2+}/TA-cal)	slope (M^{-1} s^{-1})	$k_{+2}+k_{-2}$ (s^{-1})	k_{diss} (s^{-1})	K_d (M)	F_1	F_2	F_3	F_∞
αCaMKII[a]	2.1 (±0.1) × 10^7	0.77(±0.01)	3.52 (k_{-1}) 0.343 (k_{-2})	7.47 × 10^{-8}	1	1.34	1.014	1.12
+ATP	2.1 (±0.1) × 10^7	1.0 (±0.1)	2.7 (±0.2) × 10^{-3}	1.3 × 10^{-10}	1	1.26	0.60	0.6 (±0.1)
αCaMKII[c] (Ca^{2+}/DA-cal)	nd	5.0 (±0.8)	5.83 (k_{-1}) 1.8 (±0.2) (k_{-2})	9.7 (±0.5) × 10^{-8} [b]	1	1.0	0.53	0.70(±0.15)

(Ca^{2+}/DA-cal)	slope (M^{-1} s^{-1})	$k'_{+2}+k'_{-2}$ (s^{-1})	k_{diss} (s^{-1})	K_d (M)	F_1	F'_2	F'_3	F'_∞
αCaMKII[c]								
+AMP-PNP	nd	nd	0.71(±0.05)	3.4 × 10^{-8}	1	1.0	nd	0.43(±0.03)
+ADP	1.82 (±0.04) × 10^6	>7	0.36 (±0.01)	1.7 × 10^{-8}	1	1.0	nd	0.51(±0.03)
αCaMKII + ATP	2.50 (±0.12) × 10^6	>12	≤6 × 10^{-5} [d]	≤2.8 × 10^{-12}	1	1.0	0.18	0.18(±0.02)
αCaMKII peptide Ac-294−309-NH_2[e]	1.11 (±0.02) × 10^8	>200	0.004 (±0.0005)	3.6 × 10^{-11}	1	1.0	0.18	0.18(±0.02)
αCaMKII peptide 281−319[e]	1.49 (±0.06) × 10^8	>350	0.00017 (±0.00005)	1.1 × 10^{-12}	1	1.0	0.18	0.18(±0.02)
αCaMKII peptide 281−319-Thr_{286}-P[e]	7.25 (±0.16) × 10^7	>350	0.00017 (±0.00005)	2.3 × 10^{-12}	1	1.0	0.18	0.18(±0.02)

[a] Best fit values to data in terms of Scheme 1. Values for F_3 were calculated from $F_\infty = (k_{+2}F_3 + k_{-2}F_2)/(k_{+2} + k_{-2})$ (*26*). Slope corresponds to k_{+1}. [b] K_d measured by equilibrium binding. [c] K_d corresponds to $k_{diss}/2.1 \times 10^7$. k_{diss} for Ca^{2+}/DA-cal corresponds to k_{-2}. [d] This value refers to the dissociation rate constant of Ca^{2+}/DA-cal from αCaMKII-Thr_{286}-P (Figure 2A). [e] K_d for the peptides was calculated as k_{diss}/slope. SD of linear regression (for slopes) or exponential fit (for rates) to the data is given in parentheses. SEM is given for measurements of F_∞ in steady-state measurements.

in this case, the slope, 1.8 × 10^6 M^{-1} s^{-1}, was somewhat reduced.

Ca^{2+}/DA-cal dissociation from its complex with αCaMKII was measured by displacement with pig brain Ca^{2+}/calmodulin. Upon addition of unlabeled Ca^{2+}/calmodulin, the Ca^{2+}/DA-cal fluorescence became unquenched, reaching the level of free Ca^{2+}/DA-cal fluorescence at the rate 1.8 s^{-1} (Figure 2D, record 1). Nonhydrolyzable nucleotides AMP-PNP and ADP reduced the rate of Ca^{2+}/DA-cal fluorescence increase upon displacement from the αCaMKII complex to 0.71 and 0.36 s^{-1}, respectively (records 2 and 3). Incubation of αCaMKII with ATP resulted in a marked decrease in the rate of Ca^{2+}/DA-cal dissociation such that little change was observed in 10 s (record 4). From measurement over 17 min, a rate of ≤6 × 10^{-5} s^{-1} was estimated for Ca^{2+}/DA-cal dissociation, consistent with the previously reported calmodulin trapping caused by Thr_{286}-autophosphorylation (*16*).

Mechanism of Ca^{2+}/DA-cal Interaction with αCaMKII and Its Complexes with ATP and ADP. As seen in Figure 2B, in the association with αCaMKII, Ca^{2+}/DA-cal fluorescence quenching occurred in an essentially concentration-independent manner in the range of ≤5 μM enzyme. The simplest mechanism to describe these data is a two-step process shown in Scheme 1:

Scheme 1

$$\underset{F_1}{Ca^{2+}/cal} + \alpha CaMKII \underset{k_{-1}}{\overset{k_{+1}}{\rightleftharpoons}} \underset{F_2}{Ca^{2+}/cal.\alpha CaMKII_1} \underset{k_{-2}}{\overset{k_{+2}}{\rightleftharpoons}} \underset{F_3}{Ca^{2+}/cal.\alpha CaMKII_2}$$

In terms of Scheme 1, k_{obs} corresponds to $k_{-2} + k_{+2}/(1 + k_{-1}/k_{+1}[\alpha CaMKII])$. Thus, the isomerization rate k_{obs} tends to saturate at $k_{+2} + k_{-2}$. As seen in Figure 2B, k_{obs} appears to saturate at 5.0 s^{-1}. The value for k_{-2} estimated in displacement experiments was 1.8 s^{-1}. Thus, k_{+2} corresponds to 3.2 s^{-1}. No fluorescence change appears to be associated with the initial binding of Ca^{2+}/DA-cal to αCaMKII. Ca^{2+}/DA-cal fluorescence is quenched in an isomerization process. The fluorescence of the initial Ca^{2+}/DA-cal·αCaMKII complex is thus the same as that of free Ca^{2+}/DA-cal; in terms of Scheme 1, this can be expressed as $F_1 = F_2 = 1.0$. As an estimate of the initial binding, k_{+1} of 2.1 × 10^7 M^{-1} s^{-1} is taken from experiments with Ca^{2+}/TA-cal (Figure 3). The dissociation constant, K_d, for Scheme 1 corresponds to $k_{-1}k_{-2}/k_{+1}(k_{+2} + k_{-2})$. The value of 100 nM was measured for the K_d by equilibrium binding (Figure 1B). This allows the estimation of $k_{-1} = 5.83$ s^{-1}. An F_3 of 0.53 is estimated as described in (*26*). k_{obs} values obtained by simulation of the fluorescence changes using these parameters are consistent with the data (Figure 2B, Table 2) and with the mechanism in which rapid binding is followed by slow isomerization in the interaction of Ca^{2+}/Da-cal with αCaMKII.

The kinetics of Ca^{2+}/DA-cal interaction with αCaMKII in the presence of ATP can be described by a two-step process analogous to Scheme 1. Similarly to the nucleotide-free interaction, Ca^{2+}/DA-cal binding appears to occur without a fluorescence change, with compaction occurring in an isomerization which follows the initial binding. Thus, $F_1 = F'_2 = 1.0$ and $F'_3 = 0.2$ for the ATP complex. The slope of k_{obs} in this model can be taken as the association rate constant $k'_{+1} = 2.5 \times 10^6$ M^{-1} s^{-1}. k_{obs} values measured in the association suggest that the isomerization rate $k'_{+2} + k'_{-2} > 15$ s^{-1}. Data obtained in the presence of ADP could be analyzed in a similar manner with $k'_{+1} = 1.8 \times 10^6$ M^{-1} s^{-1} (Figure 2C). k'_{-2} can be estimated from displacement reactions as 0.3 s^{-1}, and $F'_\infty = 0.5$ as measured in the steady-state. In the Ca^{2+}/DA-cal interaction with αCaMKII in the presence of ATP and ADP, the slope of k_{obs} is lower than that estimated for binding in the absence of nucleotide, and isomerization appears to be faster than binding in the concentration range studied.

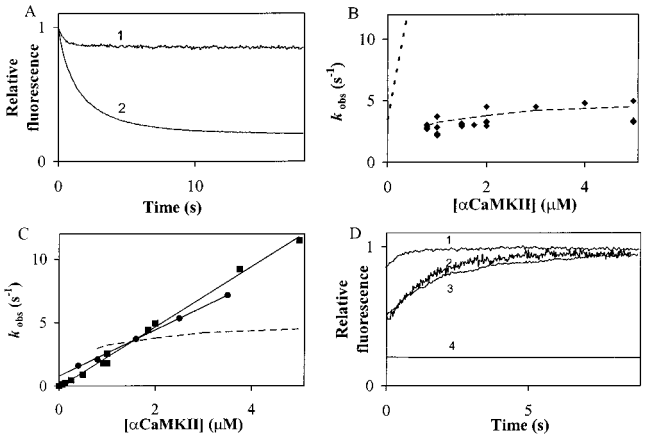

FIGURE 2: Kinetics of Ca^{2+}/DA-cal interactions with αCaMKII and nucleotides. Fluorescence stopped-flow measurements were carried out in 50 mM K-PIPES, pH 7.0, 100 mM KCl, 2 mM $MgCl_2$, 0.5 mM $CaCl_2$ at 21 °C. Concentrations are given in the mixing chamber. (A) Association kinetics of Ca^{2+}/DA-cal with αCaMKII. Record 1: Association reaction with αCaMKII. 0.2 μM Ca^{2+}/DA-cal was mixed with 1.0 μM αCaMKII. k_{obs} was 2.3 (±0.2) s^{-1}. Record 2: Association with αCaMKII in the presence of ATP. The mixture of 0.5 μM Ca^{2+}/DA-cal and 0.25 mM ATP was mixed with 0.5 μM αCaMKII. k_{obs} was 0.78 (±0.03) s^{-1}. (B) Analysis of the association kinetics of Ca^{2+}/DA-cal with αCaMKII. (◆) Plot of k_{obs} as a function of αCaMKII concentration. 0.1 or 0.2 μM Ca^{2+}/DA-cal was mixed with αCaMKII. (− −) Simulation of k_{obs} in terms of Scheme 1 using parameter values given in Table 2. (- - -) Slope 2.1×10^7 M^{-1} s^{-1} with intercept at 3.5 s^{-1} determined for Ca^{2+}/TA-cal (see Figure 3) is shown. (C) Association kinetics of Ca^{2+}/DA-cal with αCaMKII in the presence of ATP and ADP. (■) The mixture of 0.2 μM DA-cal and 0.25 mM ATP was mixed with αCaMKII. Data were best fit with slope 2.50×10^6 M^{-1} s^{-1} (solid line) with the intercept fixed at origin. (●) The mixture of 0.2 μM Ca^{2+}/DA-cal and 1.0 mM ADP was mixed with αCaMKII. Data were best fit with slope 1.82×10^6 M^{-1} s^{-1} (solid line) with the intercept at 0.8 s^{-1}. (− −) Simulated data as shown in panel B. (D) Dissociation kinetics of αCaMKII complexes of Ca^{2+}/DA-cal. Record 1: The equilibrated mixture of 0.5 μM αCaMKII and 0.5 μM Ca^{2+}/DA-cal was mixed with 2.5 μM pig brain Ca^{2+}/calmodulin. The rate of fluorescence increase was 1.8 s^{-1} starting at 0.85 relative fluorescence. Record 2: The equilibrated mixture of 0.5 μM αCaMKII, 1.25 mM AMP-PNP, and 0.2 μM Ca^{2+}/DA-cal was mixed with 2.5 μM pig brain Ca^{2+}/calmodulin. The rate of fluorescence increase was 0.71 s^{-1} starting at 0.43 relative fluorescence. Record 3: The equilibrated mixture of 0.5 μM αCaMKII, 1 mM ADP, and 0.5 μM Ca^{2+}/DA-cal was mixed with 2.5 μM pig brain Ca^{2+}/calmodulin. The rate of fluorescence increase was 0.36 s^{-1} starting at 0.51 relative fluorescence. Record 4: Dissociation kinetics of Thr_{286}-phosphorylated αCaMKII. The equilibrated mixture of 0.5 μM αCaMKII, 0.5 μM Ca^{2+}/DA-cal, and 0.25 mM ATP was mixed with 2.5 μM pig brain Ca^{2+}/calmodulin. The rate of fluorescence increase was estimated by linear extrapolation of the record over 17 min as ≤0.00006 s^{-1}.

Characterization of the Formation of the Initial Complex of αCaMKII by Ca^{2+}/TA-cal Fluorescence Changes. To understand the process of the initial binding of Ca^{2+}/calmodulin to αCaMKII in more detail, a second calmodulin probe, TA-cal, was employed. Ca^{2+}/TA-cal fluorescence changes were used in association kinetic experiments to monitor the binding process and the effect of ATP on it. The fluorescence of Ca^{2+}/TA-cal, a Lys_{75}-derivatized fluorescent calmodulin (*26*), changes in a biphasic manner on αCaMKII binding and dissociation (Figure 3A,C, Table 2). During binding, Ca^{2+}/TA-cal fluorescence initially rapidly rises and then falls in a slower process at 0.77 s^{-1}. The rate of the initial rising phase shows a linear dependence on αCaMKII concentration with a slope of 2.1×10^7 M^{-1} s^{-1} (Figure 3B). By combining this measurement with the rates of Ca^{2+}/TA-cal fluorescence changes upon its displacement from the αCaMKII complex by calmodulin (Figure 3C), the rate constants of Ca^{2+}/TA-cal interaction with αCaMKII were estimated in terms of Scheme 1 (see Table 2). Ca^{2+}/TA-cal association with αCaMKII in the presence of ATP also occurs in a biphasic reaction. As shown in Figure 3D, the initial fluorescence increase is followed by a larger decrease than in the absence of ATP to a final fluorescence of 0.5. The slow fluorescence decrease occurs at 1 s^{-1}. The rate of the initial, rising phase of Ca^{2+}/TA-cal fluorescence is, however, not affected by ATP; only the amplitude of the fluorescence rise is attenuated. Thus, ATP appears not to affect the rate of binding of Ca^{2+}/TA-cal to αCaMKII. Displacement of Ca^{2+}/TA-cal from the complex formed in the presence of ATP occurred in a markedly slower process than in the absence of ATP, with a rate of 0.003 s^{-1}. In the presence of ATP and in terms of a two-step reaction analogous to Scheme 1, $k'_{+1} = 2.1 \times 10^7$ M^{-1} s^{-1}, $k'_{+2} + k'_{-2} = 1.0$ s^{-1}, $F'_2 = 1.3$, and $F'_3 = 0.6$ are estimated (Table 2).

Characterization of the Dissociation of the Initial Complex of αCaMKII by Ca^{2+}/TA-cal Fluorescence Changes. Double-mixing displacement experiments were carried out to see how the dissociation kinetics of the initial complex were affected by ATP binding. The dissociation kinetics of the first intermediate, the Ca^{2+}/TA-cal·αCaMKII·ATP complex formed by bimolecular association, were studied by calmodulin displacement. Displacement of Ca^{2+}/TA-cal by Ca^{2+}/calmodulin was carried out at 12 °C to prevent the breakdown of ATP during the course of the experiment. First, the optimum reaction time for isolating the first intermediate was established. As shown in Figure 4A, Ca^{2+}/TA-cal fluorescence reached approximately 90% of its peak at 200 ms, at which point the following slow isomerization characterized by a decrease of fluorescence has not yet significantly progressed. It is noteworthy that at 12 °C both the association and the isomerization occurred at reduced rates; the isomerization rate was 0.07 s^{-1} (Figure 4A). The dissociation kinetics of the Ca^{2+}/TA-cal·αCaMKII complex were determined in these conditions. Ca^{2+}/TA-cal and αCaMKII were rapidly mixed, and the reaction was allowed to proceed for 200 ms. At 200 ms, displacement of Ca^{2+}/TA-cal by Ca^{2+}/calmodulin was initiated. Figure 4B shows that a biphasic fluorescence decrease occurred. The rates of the two phases were 1.47 (±0.08) and 0.17 (±0.01) s^{-1} (the ratio of their amplitudes was 0.90). Then, the dissociation kinetics of the Ca^{2+}/TA-cal·αCaMKII·ATP complex were determined. The mixture of Ca^{2+}/TA-cal and ATP was rapidly mixed with αCaMKII, and at 200 ms, displacement of Ca^{2+}/TA-cal by Ca^{2+}/calmodulin was initiated (Figure 4C). A biphasic reaction similar to that without ATP occurred. The rates of the two phases were 1.28 (±0.07) and 0.13 (±0.01) s^{-1} (the ratio of the amplitudes was 0.62). These experiments showed that the dissociation kinetics of the initial complex of Ca^{2+}/TA-cal and αCaMKII were similar with and without ATP.

Kinetics of the Interactions of Ca^{2+}/DA-cal with αCaMKII Peptides. The rates at which the distance changes between the two lobes of Ca^{2+}/calmodulin when it interacts with the target sequence may be different when peptides representing the calmodulin-binding domain are free in solution or associated with the kinase catalytic domain. To investigate

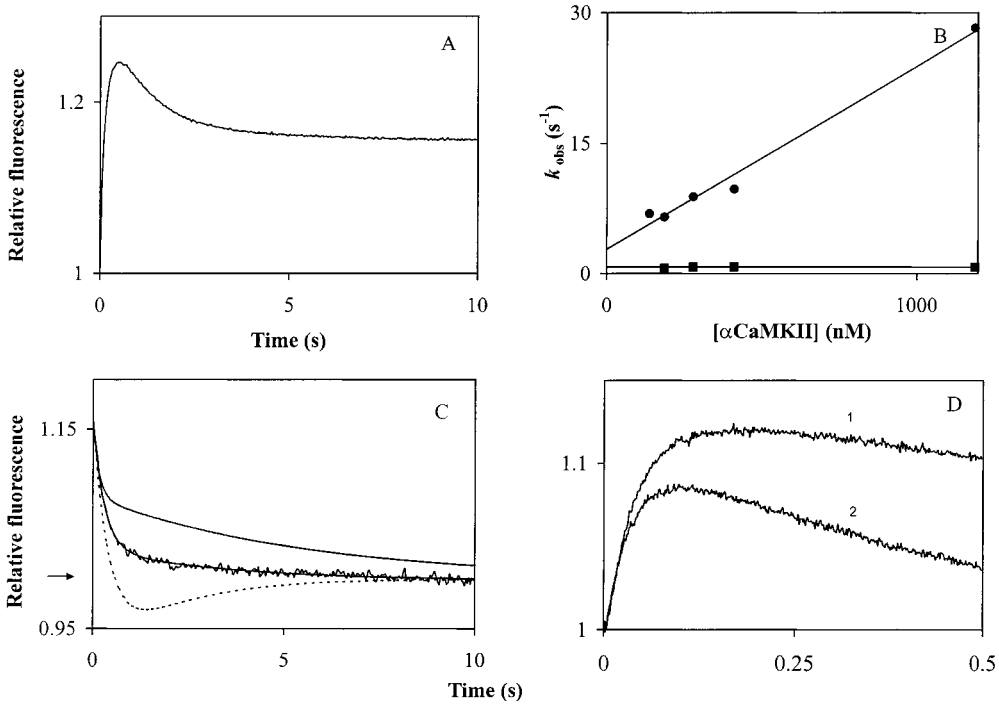

FIGURE 3: Association and dissociation kinetics of Ca^{2+}/TA-cal and αCaMKII. Fluorescence was monitored at $\lambda_{ex} = 365$ nm and $\lambda_{em} > 400$ nm, and the conditions were as described under Materials and Methods. (A) Association of Ca^{2+}/TA-cal and αCaMKII. 82 nM Ca^{2+}/TA-cal was rapidly mixed with 407 nM αCaMKII (concentrations in mixing chamber) in the stopped-flow fluorometer. The solid line shows the experimental data. The rate constants of the two exponentials shown were 9.75 s^{-1} (rising fluorescence) and 0.77 s^{-1} (decreasing fluorescence). The fluorescence started from 1 (F_1) and rose to 1.19 (F_2), and equilibrium was achieved at 1.12 (F_∞). (B) k_{obs} represents the observed rates of the fast (●) and slow (■) phases of the association reaction, an example of which is shown in panel A, plotted as a function of αCaMKII concentration. The slope of the linear regression line fit to the data (●) gave k_{+1} as 2.1×10^7 M^{-1} s^{-1} and the intercept at 2.8 s^{-1} (Scheme 1). A horizontal line drawn at 0.77 s^{-1} marks the mean value of the data (■) at [αCaMKII] >400 nM to define $k_{obs} = k_{+2} + k_{-2}$ as 0.77 s^{-1}. (C) Displacement of Ca^{2+}/TA-cal by Ca^{2+}/calmodulin from its complex with αCaMKII. The equilibrated mixture of 41 nM Ca^{2+}/TA-cal and 205 nM αCaMKII was rapidly mixed with 1.5 μM calmodulin (mixing chamber concentrations). A biphasic fluorescence decrease occurred (the arrow points to fluorescence intensity 1). The exponential rate of the first phase was 3.33 s^{-1}, and that of the second phase was 0.36 s^{-1}. The ratio of the amplitudes of the two exponentials was $F_r = 4.8$. Using the observed rate and fluorescence values, the rate constants and fluorescences of the two Ca^{2+}/TA-cal·αCaMKII complexes were determined in terms of a two-step reaction in which rapid binding is followed by isomerization (*26*). The experimental record was overlayed with a solid line generated using the calculated values (line 1 through data): $k_{-1} = 3.52$ s^{-1}; $k_{+2} = 0.427$ s^{-1}; $k_{-2} = 0.343$ s^{-1}; $F_3 = 1.104$ (Table 1). Line 2 was generated by setting k_{-1} to 0.35 s^{-1}, and so $k_{+2} = 0.20$ s^{-1}, $k_{-2} = 0.57$ s^{-1}, and $F_3 = 0.647$ followed. For line 3, k_{-1} was set to 6.0 s^{-1}, and so $k_{+2} = 0.57$ s^{-1}, $k_{-2} = 0.20$ s^{-1}, and $F_3 = 1.097$ followed. $k_{+1} = 0$ and $F_2 = 1.34$ were used throughout the simulations. (D) Initial rapid phase of Ca^{2+}/TA-cal fluorescence changes. 1.08 μM αCaMKII was rapidly mixed with 33.2 nM Ca^{2+}/TA-cal (record 1) and with the mixture of 0.5 mM ATP and 33.2 nM Ca^{2+}/TA-cal (record 2). The fluorescence initially rose to 1.10 and 1.041, respectively. The exponential rates were fit to 28.3 and 37.5 s^{-1}. This difference, however, likely reflects the effect of ATP on the amplitude rather than the rate of the initial Ca^{2+}/TA-cal fluorescence rise in association with αCaMKII.

this, the interactions of αCaMKII-derived calmodulin-binding peptides with Ca^{2+}/DA-cal were studied in stopped-flow experiments. As shown in Figure 5A, in the association of Ca^{2+}/DA-cal with the Ac-294−309-NH_2 peptide, maximum quenching occurred. The fluorescence decay was rapid and could be described by a single exponential. Similar observations were made with the 281−319 and 281−319-Thr_{286}-P peptides as well. For each peptide, the observed rates were rapid, in excess of 200 s^{-1}, and showed a linear dependence on the peptide concentration (Figure 5B). The slopes were 1.1×10^8, 1.5×10^8, and 0.7×10^8 M^{-1} s^{-1} for peptides Ac-294−309-NH_2, 281−319, and 281−319-Thr_{286}-P, respectively.

Upon displacement of Ca^{2+}/DA-cal from its peptide complexes by unlabeled Ca^{2+}/calmodulin, the fluorescence quenching was reversed. The dissociation rate of Ca^{2+}/DA-cal from its complex with the Ac-294−309-NH_2 peptide was 4.0×10^{-3} s^{-1} (Figure 5C, record 1). The displacement of Ca^{2+}/DA-cal from its complexes with αCaMKII peptides 281−319 and 281−319-Thr_{286}-P occurred at the lower rate of 1.7×10^{-4} s^{-1} (Figure 5C, record 2 shows the Ca^{2+}/DA-cal fluorescence change upon 281−319-Thr_{286}-P peptide dissociation). In terms of Scheme 1, the following values are consistent with our data: $k_{+1} = 10^8$ M^{-1} s^{-1}; $k_{+2} > 350$ s^{-1}; $k_{-2} \leq 4 \times 10^{-3}$ s^{-1}; $F_1 = F_2 = 1.0$; and $F_3 = 0.2$ (Table 2).

DISCUSSION

DA-cal, a Probe of Overall Calmodulin Conformation. Our distance estimates by FRET can be compared with distances in the crystal structures of calmodulin and its complex with an αCaMKII target peptide. The distance between the chomophore pair labeling the C34 and C110 residues located on each of the two Ca^{2+}-binding lobes of calmodulin by FRET was estimated as 22 Å in a target peptide complex of Ca^{2+}/calmodulin in solution. The distance between the C_α atoms of residues T34 and T110 in the Ca^{2+}/calmodulin complex of a similar αCaMKII target peptide is 15 Å (*19*). In comparing the two types of estimate, the length of the Cys side chain and the probe dimensions have to be

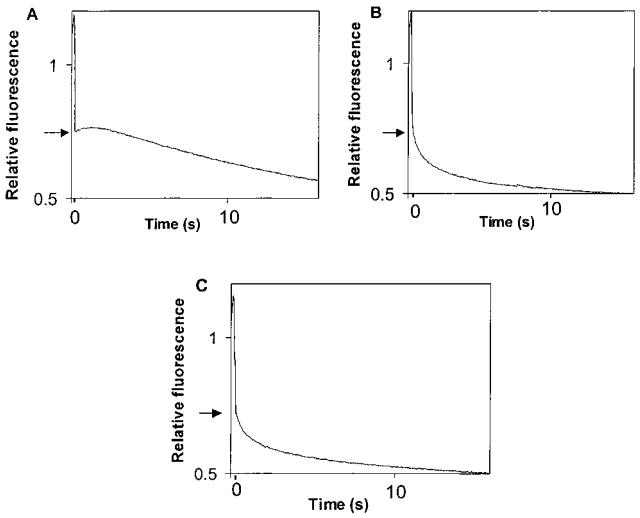

FIGURE 4: Ca^{2+}/TA-cal dissociation kinetics from αCaMKII·ATP complex by double-mixing stopped-flow. All the reactions were carried out at 12 °C to reduce ATP hydrolysis during the experiment. 100 nM Ca^{2+}/TA-cal solution was rapidly mixed with 1.08 μM αCaMKII. This first mixture was mixed with buffer or 2 μM Ca^{2+}/calmodulin after a 200 ms delay time which was required to allow the first phase of the association process to go to 90% completion. Time 0 indicates the time of the second mixing. (A) Control for Ca^{2+}/TA-cal displacement with buffer. The mixture of TA-cal and αCaMKII was mixed with buffer at 200 ms. As seen in the record, after the first mixing step, the fluorescence of the initial complex with αCaMKII appears; at 200 ms, the fluorescence is rapidly reduced by dilution with buffer, and the slow decreasing phase of the fluorescence change occurs. (B) Displacement of Ca^{2+}/TA-cal from complex with αCaMKII. The first mixture of TA-cal and αCaMKII was mixed with calmodulin at 200 ms. After the rapid drop of fluorescence by the second mixing, the fluorescence decay indicates TA-cal dissociation in a biexponential process with rates 1.50 and 0.17 s^{-1} (amplitude ratio 0.9). Note that these rates are slower than those shown in Figure 4, where the experiments were carried out at 21 °C. (C) Displacement of Ca^{2+}/TA-cal from complex with αCaMKII·ATP. The first mixture of TA-cal and αCaMKII in the presence of 100 μM ATP was mixed with calmodulin at 200 ms. A fluorescence change similar to that in panel B occurred, and the biexponential fluorescence decay was fit with rates 1.37 and 0.13 s^{-1} (amplitude ratio 0.62). In further experiments (not shown), ATP concentrations up to 2 mM were used. At 2 mM ATP, the rates were reduced to 1.04 and 0.11 s^{-1} (amplitude ratio 0.49). This was most likely due to the presence of 1−5% ADP in the ATP sample.

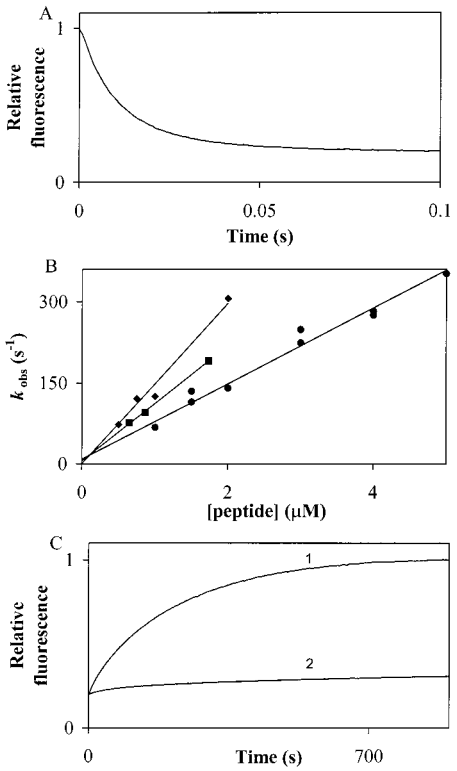

FIGURE 5: Kinetics of Ca^{2+}/DA-cal interaction with αCaMKII-derived peptides. (A) Association of Ca^{2+}/DA-cal with Ac-294−309-NH_2 peptide. 0.5 μM Ca^{2+}/DA-cal was mixed with 0.65 μM Ac-294−309-NH_2 peptide. k_{obs} was 87 s^{-1}. (B) Association kinetics. 0.2 μM Ca^{2+}/DA-cal was mixed with peptide. (■) Ca^{2+}/DA-cal association with Ac-294−309-NH_2 peptide. The slope of the linear fit to the data points was 1.1×10^8 M^{-1} s^{-1}; the intercept was at 5.0 s^{-1}. (◆) Ca^{2+}/DA-cal association with 281−319 peptide. The slope of the linear fit to the data points was 1.5×10^8 M^{-1} s^{-1}, and the intercept was fixed at origin. (●) Ca^{2+}/DA-cal association with 381−319-Thr_{286}-P peptide. The slope of the linear fit to the data points was 0.7×10^8 M^{-1} s^{-1}. The intercept was at 8.5 s^{-1}. (C) Dissociation kinetics. Record 1: The equilibrated mixture of 0.65 μM Ac-294−309-NH_2 peptide and 0.5 μM Ca^{2+}/DA-cal was mixed with 2.5 μM pig brain Ca^{2+}/calmodulin. The rate of fluorescence increase was 0.004 s^{-1}. Record 2: Dissociation kinetics of 281−319-Thr_{286}-P peptide. The equilibrated mixture of 0.5 μM 281−319-Thr_{286}-P peptide and 0.2 μM Ca^{2+}/DA-cal was mixed with 2.5 μM pig brain Ca^{2+}/calmodulin. The rate of fluorescence increase was estimated at 0.00017 s^{-1} by linear extrapolation.

taken into account. The labeled SH- groups are each located approximately 3 Å from the C_α atoms. The distance between the center of the probe and the SH- group is 10 Å for the dansyl group and 6 Å for DDP (*22*). Thus, in an extreme case, the Cys side chain and probe sizes may account for an additional 22 Å in the measured distance. The probe dimensions thus are likely to contribute to our 7 Å greater distance estimate for the peptide complex compared to the crystal structure.

The C_α atoms of T34 and T110 are 50 Å apart in the crystal structure of Ca^{2+}/calmodulin (*21*). Given the estimated R_o value of 26 Å for DA-cal, the transfer efficiency is <0.08 at distances greater than 39 Å, and such distances are thus less accurately estimated by this probe. The FRET measurements showing two Ca^{2+}/DA-cal conformers in solution with interprobe distances of 40−45 and 28 Å are nonetheless consistent with the more dynamic and somewhat collapsed structure of Ca^{2+}/calmodulin in solution compared to that in the crystal (*20*, *39*).

The critical distance was estimated using the value 2/3 for the orientation factor κ^2 assuming full rotational flexibility of the probes (*37*). This assumption is commonly made in this type of measurement as κ^2 is not readily determined experimentally. We considered the fluorescence properties of the donor to assess the validity of this assumption. The relatively short 12−15 ns lifetime of AEDANS-T34C/T110C-calmodulin and the relatively low quantum yield of the AEDANS fluorophore attached to T34C/T110C-calmodulin (Table 1) are consistent with the probe being exposed to the aqueous medium and thus possessing rotational flexibility. Steady-state anisotropy measurements showed that AEDANS attached to T34C/T110C-calmodulin had low anisotropy, approximately 0.02, and changes little (by <0.05) in the presence of Ca^{2+} and the other ligands. Thus, even though its exact value remains uncertain, κ^2 does not appear to be significantly affected by these protein interactions, and the assumption of $\kappa^2 = 2/3$ seems reasonable for our system.

Multiple Ca^{2+}/DA-cal Structures in Complex with αCaMKII. At least two classes of Ca^{2+}/calmodulin conformer are reported by Ca^{2+}/DA-cal upon interaction with αCaMKII. Initial binding appears to occur with little or no fluorescence change in Ca^{2+}/DA-cal, indicating binding in extended conformation retaining the dynamic distribution of Ca^{2+}/calmodulin conformers. It is likely that this type of Ca^{2+}/calmodulin binding occurs by attachment by one lobe only (*40, 41*). Nucleotide binding and Thr_{286}-autophosphorylation cause compaction of bound Ca^{2+}/calmodulin structure. Substantial Ca^{2+}/calmodulin conformation change appears to occur upon nucleotide binding to αCaMKII without Thr_{286}-autophosphorylation. When Ca^{2+}/DA-cal is bound to ADP- and AMP-PNP complexes of αCaMKII, fluorescence quenching is intermediate. It should be borne in mind that steric restriction of the freedom of movement of the probes may occur independently of further compaction of Ca^{2+}/DA-cal. Alternatively, in these complexes, Ca^{2+}/calmodulin conformation may be more compact and/or the equilibrium between the initial and the compacted complexes is shifted toward the compacted form. Ca^{2+}/calmodulin conformation appears maximally compact when bound to αCaMKII-Thr_{286}-P and to αCaMKII peptides Ac-294−309-NH_2, 281−319, and its Thr_{286}-phospho analogue. Our results described here for αCaMKII represent the first case in which multiple Ca^{2+}/calmodulin conformations associated with the regulation of activity have been identified in a target enzyme. Putative Ca^{2+}/calmodulin·αCaMKII conformers are diagrammatically illustrated in Figure 6.

Stoichiometry and Cooperativity. αCaMKII exists as an oligomeric complex of 12 subunits (*11*−*13*). Activation by Ca^{2+}/calmodulin, nucleotide binding, and autophosphorylation are all to some extent cooperative, although the level of cooperativity is still a matter of debate (*1* and references cited within, *17*). Potential cooperativity and the precise stoichiometry of the Ca^{2+}/calmodulin transitions observed here are difficult to establish. Thus, the observed interaction between nucleotide and Ca^{2+}/calmodulin binding does not necessarily require these ligands to be bound to the same monomer or to be bound with equal stoichiometries. Such effects would produce a set of subpopulations of the intermediate states deduced from our kinetic analysis. However, we have no evidence for such subpopulations from our analysis. This would suggest either that the level of cooperativity is quite small or that individual subpopulations have similar behavior with regard to their interaction with Ca^{2+}/calmodulin. Hence, for simplicity and clarity, cooperative interactions are not included in our current model.

Mechanism of Ca^{2+}/Calmodulin Binding to αCaMKII Peptides. Each peptide caused maximum quenching of Ca^{2+}/DA-cal fluorescence, indicating that Ca^{2+}/DA-cal conformation was compact in each complex. The linear concentration dependence of the Ca^{2+}/DA-cal conformational change in the association process with αCaMKII peptides suggests that the Ca^{2+}/DA-cal conformational transition from extended to compact is faster than the binding in the concentration range studied. This behavior is similar to the corresponding interactions with αCaMKII induced by nucleotides except that the compaction rate is greatly enhanced with the peptides. Similar observations were made in the interaction of Ca^{2+}/DA-cal with MLCK and its Ca^{2+}/calmodulin-binding peptide, where rapid >50 s^{-1} Ca^{2+}/calmodulin compaction was seen in a concentration-dependent manner (*24*). This observation can be viewed as initial Ca^{2+}/DA-cal binding without a fluorescence change followed by rapid compaction in an isomerization of the initial complex. Thus, the initial binding of Ca^{2+}/calmodulin to peptides may occur with one lobe only as proposed here for the αCaMKII enzyme. A similar model has been proposed for the interaction of Ca^{2+}/calmodulin with MLCK (*40, 41*).

The rate of Ca^{2+}/calmodulin compaction is >350 s^{-1}, and the rate of its reversal for Ac-294−309-NH_2 is 0.004 s^{-1}; thus, $>8.75 \times 10^4$-fold stabilization of Ca^{2+}/calmodulin binding occurs in the calmodulin compaction that follows initial binding. This factor is $>2 \times 10^6$ for the 281−319 peptide and its Thr_{286}-phospho analogue. The kinetic and energetic differences between the interaction of peptides and intact αCaMKII with Ca^{2+}/calmodulin may be explained by the attachment of the autoinhibitory and contiguous Ca^{2+}/calmodulin-binding domain to the catalytic core, thereby restricting its folding. Previous studies using a fluorescently labeled K75C-calmodulin mutant showed marked differences in the dissociation between peptide complexes and suggested that residues 293−295 markedly stabilize Ca^{2+}/calmodulin binding (*42*). Our dissociation data with Ca^{2+}/DA-cal and similar peptides gave equivalent results.

Stabilization of Ca^{2+}/Calmodulin Binding to αCaMKII by Nucleotides. It has previously been shown that Ca^{2+}/calmodulin binding increases the ADP binding affinity for brain CaMKII (*43*). Here we observe that nucleotides such as ADP and AMP-PNP increase the Ca^{2+}/calmodulin binding affinity for αCaMKII. Our data suggest that stabilization of Ca^{2+}/calmodulin binding occurs in the isomerization that follows the initial binding. Isomerization of αCaMKII-bound Ca^{2+}/DA-cal from extended to compact becomes >2-fold more rapid, and Ca^{2+}/DA-cal dissociation occurs at a 5-fold lower rate in the presence of ADP, resulting in a >10-fold stabilization of Ca^{2+}/calmodulin binding to αCaMKII. Nucleotides have a substantial effect on the mechanism of interaction of Ca^{2+}/calmodulin and αCaMKII in that binding becomes rate-limiting to the isomerization of Ca^{2+}/calmodulin, making it closer to the behavior with target peptides.

Mechanism of αCaMKII Activation by Ca^{2+}/Calmodulin and ATP. We consider our data in the framework of a two-substrate reaction in which the ternary complex may in principle be generated either by random or by compulsory order mechanisms by pathway A or B (Figure 6). Ca^{2+}/calmodulin initially binds in extended conformation to αCaMKII or to αCaMKII·ATP to form a ternary complex (species 3a). Ca^{2+}/calmodulin compaction is postulated to occur by rapid isomerization of species 3a to species 4a followed by Thr_{286}-autophosphorylation as transition 4a → 4b. Ca^{2+}/calmodulin binding to nucleotide-free αCaMKII corresponding to the transition of species 1 → 2a → 2b is analyzed in terms of Scheme 1 above. The existence of ATP-bound αCaMKII in the absence of Ca^{2+}/calmodulin has been demonstrated by Ca^{2+}/calmodulin-independent autophosphorylation of αCaMKII with a K_m 145 μM for ATP (*44*).

When comparing the association kinetics of Ca^{2+}/DA-cal and Ca^{2+}/TA-cal in the presence of ATP, a paradox arises: while Ca^{2+}/calmodulin binding to αCaMKII appears to be rapid with rate constant $k_{+1} = 2.1 \times 10^7$ M^{-1} s^{-1} with or without ATP (Figure 3), the net rate of Ca^{2+}/calmodulin

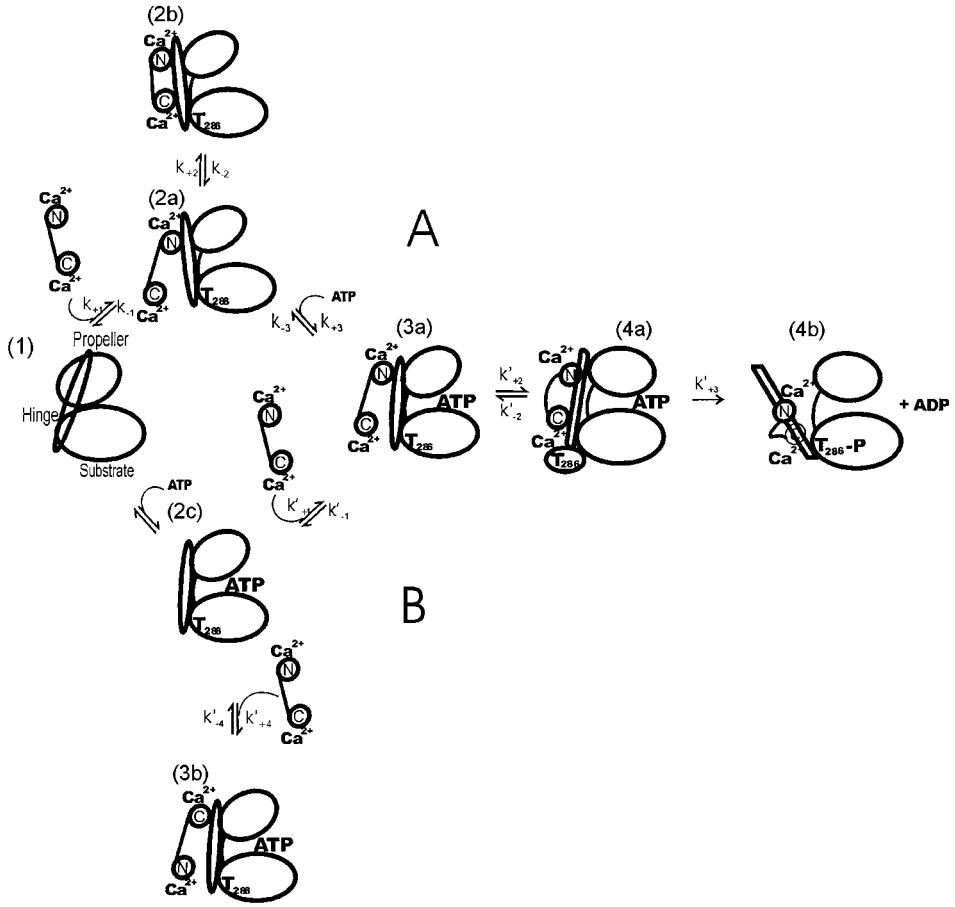

FIGURE 6: Diagrammatic representation of Ca^{2+}/calmodulin conformers in αCaMKII complexes in a putative activation scheme. A typical kinase catalytic domain is illustrated by ellipsoids representing the two core domains termed 'propeller' and substrate. Nucleotide binds in the cleft formed by the two core domains linked by a hinge region (*45*). The autoinhibitory and contiguous Ca^{2+}/calmodulin binding domain is represented by an elongated ellipsoid. On the basis of sequence homologies and crystallographic data with CaMKI (*9*) and titin kinase (*46*), it is supposed that this region in αCaMKII also adopts α-helix−loop−α-helix fold, termed the αR1−loop−αR2 motif (*9*). In our illustration, transition from ellipsoid to cylindrical appearance indicates increased α-helical content of the calmodulin binding region. Three classes of αCaMKII-bound Ca^{2+}/calmodulin conformation are represented. The first class is extended (intermediates 2a, 3a, and 3b). Species 2a and 3a are on the activation path; 3b, however, represents a putative dead-end complex. Possible structural explanations for the unproductive nature of a dead-end complex are that ATP binding (1) restricts Ca^{2+}/calmodulin binding to an inhibitory site (*47*) or (2) causes Ca^{2+}/calmodulin binding in an incorrect orientation and that (3) Ca^{2+}/calmodulin is attached via the wrong lobe. For the purpose of illustration, only the latter option is depicted. The second class of αCaMKII-bound Ca^{2+}/calmodulin conformers adopts a semi-compact conformation. Such conformation is observed in species 2b and probably 4a. This conformer is depicted with a reduced distance between the Ca^{2+} binding lobes. Semi-compact conformations may occur by partial helical folding of the calmodulin binding region, and this is indicated in the diagram by depicting the autoinhibitory and calmodulin binding region as a cylinder. In species 4a, ATP binding to the Ca^{2+}/cal complex of αCaMKII stabilizes an intermediate in which Thr_{286} is accessible for autophosphorylation. It must be noted that the precise conformation of Ca^{2+}/calmodulin in the Ca^{2+}·cal·αCaMKII·ATP complex (species 4a) could not be determined by either our equilibrium or transient kinetic studies. The third class of αCaMKII-bound Ca^{2+}/calmodulin conformation is maximally compact. Such a conformation is observed by energy transfer measurements in Ca^{2+}/DA-cal complexes with αCaMKII peptides Ac-294−309-NH_2, 281−319, and 281−319-Thr_{286}-P as well as in species 4b in the diagram. Our data thus suggest that, as in peptide complexes (*48*), maximally compact calmodulin conformation in complex with Thr_{286}-phospho-αCaMKII is accomplished when the calmodulin binding region in the enzyme is stabilized as an α-helix. We postulate that when Ca^{2+}/calmodulin conformation is extended or semi-compact, the attachments of the autoinihibitory and calmodulin binding region to the catalytic core are not completely abolished. However, when Ca^{2+}/calmodulin conformation is maximally compact, in Thr_{286}-phospho-αCaMKII, the calmodulin binding domain may be detached from the catalytic core.

compaction observed in the presence of ATP (or ADP) is described by a lower slope of $k'_{+1} = 2 \times 10^6\ M^{-1}\ s^{-1}$ (Figure 2C). The lower slope compared to the binding and concentration dependence of Ca^{2+}/calmodulin compaction could in principle be explained if the initial Ca^{2+}/cal binding to αCaMKII is destabilized by ATP such that the Ca^{2+}/cal dissociation rate from the initial Ca^{2+}/cal·αCaMKII·ATP complex is greatly increased. However, double-mixing displacement experiments comparing Ca^{2+}/TA-cal dissociation from the initial complexes formed in the absence and presence of ATP (Figure 4) showed no such effect. Alternatively, the kinetic effects of ATP can be explained by an apparent reduction by ATP in the concentration of αCaMKII available for Ca^{2+}/calmodulin compaction. Such an effect would be the result of the formation of unproductive as well as productive Ca^{2+}/cal·αCaMKII·ATP complexes. Species 3b represents such a complex in which incorrectly bound Ca^{2+}/calmodulin is illustrated for the purpose of the argument (Figure 6). In our illustration, this complex is linked to the general scheme by Ca^{2+}/calmodulin dissociation, a process which may be significant in our experimental conditions of saturating ATP and limiting Ca^{2+}/calmodulin concentrations.

Such a dead-end complex is characteristic of compulsory order ligand-binding mechanisms.

In summary, at least two αCaMKII-bound Ca^{2+}/calmodulin-binding conformations are demonstrated. Ca^{2+}/calmodulin binding is required for kinase activity; however, it appears that ATP binding is necessary for the stabilization of bound Ca^{2+}/calmodulin. These two ligands together, thus, appear to induce enzyme conformational changes which are not generated by either ligand alone.

REFERENCES

1. Schulman, H., and Braun, A. (1999) in *Calcium as Cellular Regulator* (Carafoli, E., and Klee, C. B., Eds.) pp 311−343, Oxford University Press, New York.
2. Strack, S., Choi, S., Lovinger, D. M., and Colbran, R. J. (1997) *J. Biol. Chem. 272*, 13467−13470.
3. Shen, K., Teruel, M. N., Connor, J. H., Shenolikar, S., and Meyer, T. (2000) *Nat. Neurosci. 9*, 881−886.
4. McGlade-McCulloh, E., Yamamoto, H., Tan, S.-E., Brickey, D. A., and Soderling, T. R. (1993) *Nature 362*, 640−642.
5. Derkach, V., Barria, A., and Soderling, T. R. (1999) *Proc. Natl. Acad. Sci. U.S.A. 96*, 3269−3274.
6. Malenka, R. C., Kauer, J. A., Perkel, D. J., Mauk, M. D., Kelly, P. T., Nicoll, R. A., and Waxham, M. N. (1989) *Nature 340*, 554−557.
7. Bliss, T. V. P., and Collinridge, G. L. (1993) *Nature 361*, 31−39.
8. Mayford, M., Bach, M. E., Huang, Y.-Y., Wang, L., Hawkins, and Kandel, E. R. (1996) *Nature 274*, 1678−1682.
9. Goldberg, J., Nairn, A. C., and Kuriyan, J. (1996) *Cell 84*, 875−887.
10. Woodgett, J. R., Davison, M. T., and Cohen, P. (1983) *Eur. J. Biochem. 136*, 481−487.
11. Török, K., and Morris, E. P. (1996) *Biophys. J. 70*, A58.
12. Kolodziej, S. J., Hudmon, A., Waxham, N. M., and Stoops, J. K. (2000) *J. Biol. Chem. 275*, 14354−14359.
13. Morris, E. P., and Török, K. (2001) *J. Mol. Biol. 308*, 1−8.
14. Kanaseki, T., Ikeuchi, Y., Sugiura, H., and Yamauchi, T. J. (1991) *J. Cell Biol. 115*, 1049−1060.
15. Miller, S. G., Patton, B. L., and Kennedy, M. B. (1988) *Neuron 1*, 593−604.
16. Meyer, T., Hanson, P. I., Stryer, L., and Schulman, H. (1992) *Science 256*, 1199−1202.
17. Miller, S. G., and Kennedy, M. B. (1986) *Cell 44*, 861−870.
18. Braun, A. P., and Schulman, H. (1995) *Annu. Rev. Physiol. 57*, 417−445.
19. Meador, W. E., Means, A. R., and Quiocho, F. A. (1993) *Science 262*, 1718−1721.
20. Wall, M. E., Clarage, J. B., and Phillips, G. N., Jr. (1997) *Structure (London) 5*, 1599−1612.
21. Chattopadhyaya, R., Meador, W. E., Means, A. R., and Quiocho, F. A. (1992) *J. Mol. Biol. 228*, 1177−1192.
22. Dalbey, R. E., Weiel, J., and Yount, R. G. (1983) *Biochemistry 22*, 4696−4706.
23. O'Hara, P. B., Mabuchi, Y., and Grabarek, Z. (1994) *Biophys. J. 66*, A58.
24. Török, K., and Grabarek, Z. (1998) *Biophys. J. 74*, A152.
25. Drum, C. L., Yan, S.-Z., Sarac, R., Mabuchi, Y., Beckingham, K., Bohm, A., Grabarek, Z., and Tang, W.-J. (2000) *J. Biol. Chem. 275*, 36334−36340.
26. Török K., and Trentham, D. R. (1994) *Biochemistry 33*, 12807−12820.
27. Török, K., Stauffer K., and Evans, W. H. (1997) *Biochem. J. 326*, 479−483.
28. Török, K., Wilding, M., Groigno, L., Patel, R. D., and Whitaker, M. J. (1998) *Curr. Biol. 8*, 692−699.
29. Li, C.-J., Heim, R., Lu, P., Pu, Y., Tsien, R. Y., and Chang, D. C. (1999) *J. Cell Sci. 112*, 1567−1577.
30. Brickey, D. A., Colbran, R. J., Fong, Y.-L., and Soderling, T. R. (1990) *Biochem. Biophys. Res. Commun. 173*, 578−584.
31. Török, K., Cowley, D. J., Brandmeier, B. D., Howell, S., Aitken, A., and Trentham, D. R. (1998) *Biochemistry 37*, 6188−6198.
32. Towbin, H., Staehelin, T., and Gordon, J. (1979) *Proc. Natl. Acad. Sci. U.S.A. 76*, 4350.
33. Tan, L. J., Ravid, S., and Spudich, J. A. (1992) *Annu. Rev. Biochem. 61*, 721−759.
34. Rowe, T., and Kendrick-Jones, J. (1992) *EMBO J. 11*, 4715−4722.
35. Gill, S. C., and von Hippel, P. H. (1989) *Anal. Biochem. 182*, 319−326.
36. Bradford, M. M. (1976) *Anal. Biochem. 72*, 248−254.
37. Fairclough, R. H., and Cantor, C. R. (1978) *Methods Enzymol. 28*, 347−379.
38. Tao, T., and Cho, J. (1979) *Biochemistry 18*, 2759−2765.
39. Török, K., Lane, A. N., Martin, S. R., Janot, J.-M., and Bayley, P. M. (1992) *Biochemistry 31*, 3452−3462.
40. Bayley, P. M., Findlay, W. A., and Martin, S. R. (1996) *Protein Sci. 5*, 1215−1228.
41. Persechini, A., Yano, K., and Stemmer, P. M. (2000) *J. Biol. Chem. 275*, 4199−4204.
42. Waxham, M. N., Tsai, A.-L., and Putkey, J. A. (1998) *J. Biol. Chem. 273*, 17579−17584.
43. Kwiatkowski, A. P., and King, M. (1987) *Biochemistry 26*, 7636−7640.
44. Colbran, R. J. (1993) *J. Biol. Chem. 268*, 7163−7170.
45. Johnson, L. N., Lowe, E. D., Noble, M. E. M., and Owen, D. J. (1998) *FEBS Lett. 430*, 1−11.
46. Mayans, O., van der Ven, P. F. M., Wilm, M., Mues, A., Young, P., Furst, D. O., Wilmanns, M., and Gautel, M. (1998) *Nature 395*, 863−869.
47. Krueger, J. K., Gallagher, S. C., Zhi, G., Geguchadze, R., Persechini, A., Stull, J. T., and Trewhella, J. (2001) *J. Biol. Chem. 276*, 4535−4538.
48. Brokx, R. D., Lopez, M. M., Vogel, H. J., and Makhatadze, G. I. (2001) *J. Biol. Chem. 276*, 14083−14091.
49. Wolff-Long, V. L., Tao, T., and Lowey, S. (1995) *J. Biol. Chem. 270*, 31111−31118.

BI010920+